Some Advantages of Using Bi-directional S-Parameters in Near-Field Measurements[1]

David R. Novotny, Alex J. Yuffa, Ronald C. Wittmann, Michael H. Francis, Joshua A. Gordon
Communications Technology Laboratory
National Institute of Standard and Technology
Boulder, Colorado, United States of America
david.novotny@nist.gov

***Abstract*—The unknown-thru calibration technique is being used to achieve a system level calibration at millimeter wave frequencies (>50 GHz) on the robotic ranges at NIST. This two-port calibration requires the use of a full bi-directional measurement, instead of a traditional single-direction antenna measurement. We explored the value of the additional data acquired. We find that we can use this information to verify antenna/scan alignment, image the scattering from the positioner/facility, and perform a first order correction to the transmission data for uncertainties due to LO cable flexure.**

I. Introduction

It has been shown that vector network analyzers (VNA) can be used to great effect in antenna measurements [1,2]. However, in most production antenna scanning applications, measurement speed and costs are usually overarching concerns. Bi-directional calibrations and scans with a network analyzer take longer than conventional measurement receivers because at least twice the number of measurements and four times the data are required in comparison to the single-direction case. These measurements must be taken at different times to isolate the forward and reverse scattering parameters. Such measurements take more time and require more resources, system drift can increase with longer operational times and space-time coordination between the forward and reverse measurements can complicate processing.

Despite the many operational drawbacks, a fully calibrated bi-directional system can reveal information on antenna-to-antenna interaction (is the scan too close), real-time drift checks for cable bending or other environmental changes. The redundant measurements can also provide a consistency check. When using broad frequency sweeps, we can use software position correction to compensate for the moving probe results. Then we might use more tools, like time domain gating, to examine and remove extra reflections, back image to the antenna-under-test (AUT) to assess scan alignment and see changes in horn reflections.

We hope to show that the extra effort and resources associated with this measurement might lead to some advantages in situations where lower uncertainty measurements are desired.

II. CROMMA and the Unkown Thru

The Configurable Robotic Millimeter Antenna (CROMMA) facility, Figure. 1, is based on two robotic structures [3]: the probe positioner is a six degree of freedom (DoF) serial robotic arm with 15 μm resolution. The antenna under test (AUT) positioner is a parallel hexapod positioner with 0.2 μm resolution. These motion stages are guided by a laser tracker with ~10 μm accuracy. This resolution is acceptable for positioning antennas, but it is larger than the 3 μm machining tolerances specified in the UG-385/U connector specification. Further exacerbating the situation, the RF hardware is mechanically linked to several large and heavy (~ 10 kg) laser tracker targets, so precise connections for calibration and normalization, are difficult.

Since we cannot perform a robotic-guided mechanical connection between the robotic arm and the hexapod mounted equipment, we use the unknown-thru calibration to characterize and remove the systematic effects of the VNA from the desired transmission between the antennas. The unknown-thru requires a full reflection calibration on each port, which establishes the port-to-samplers' loss and phase relation for each port [4,5]. A reciprocal thru and a frequency spacing that avoids aliasing in the electrical length of the unknown-thru is needed to establish the relative phase relations between the samplers.

Assuming reciprocity between the ports and through the antennas, *i.e.* $S_{21}=S_{12}$, this allows us to calibrate each port and perform a "thru" given a minimal loss (< 30 dB) between the probe and AUT. The robots are sufficiently accurate that the "unknown-thru" reference point can be repeated to less than 30 μm, better than λ/80 for these tests, and be used as a drift check and re-calibration point during the measurements.

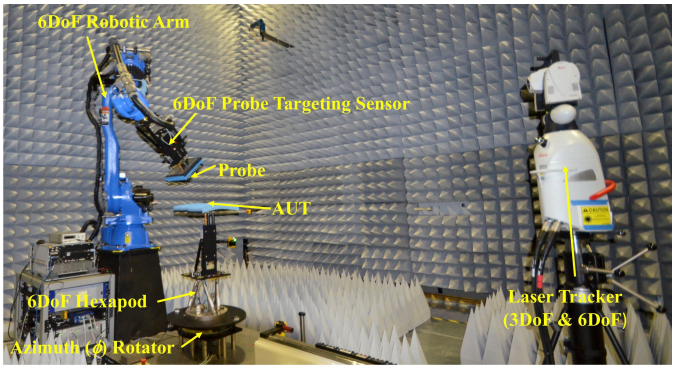

Figure 1. The CROMMA facility installed at NIST.

A. Antennas

We characterized a WR-08 system feed horn operating across a frequency range of 112–125 GHz [6,7]. To characterize the radiation from the AUT, we performed a three-antenna gain extrapolation with the AUT (a WR-08 feed horn), the probe (a μ=±1 antenna), and a 15 dBi pyramidal horn. The on-axis gains were determined via the extrapolation method [8]. Then the far-field (FF) pattern measurements were performed on the probe, using the pyramidal horn. Finally, spherical near-field (SNF) scans of AUT were performed using the probe.

B. Idealized S-parameters

One issue with using remote mixing and fully bi-directional measurements is that there are multiple ways to introduce errors. In Figure 2, we see a block diagram of the VNA setup. Changes in the local oscillator (LO) cable, C_{LO1}, affects primarily waves a_1 and b_1, while changes in C_{LO2} affects waves a_2 and b_2. If harmonic mixers are used, changes in the LO signals at the mixers may not linearly transfer through the mixers.

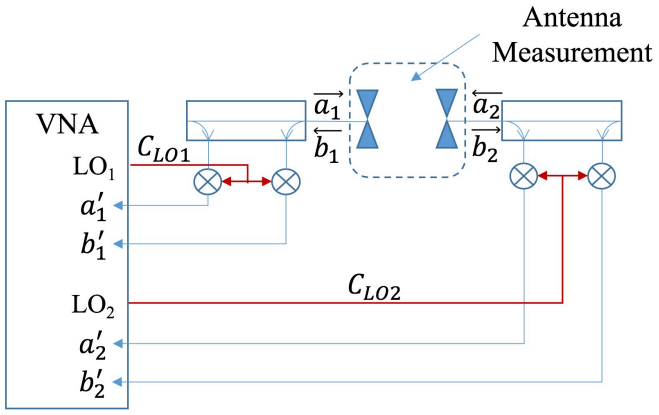

Figure 2. Simplified signal block diagram for a bi-directional frequency-converting two-port VNA measurement. The source is not shown as changes in the source signal are minimized by the ratioed nature of the S-parameter measurement.

If Figure 2 is idealized by perfect couplers, ideal and balanced mixers and matched interfaces, we can assume that the received wave parameters a_1', b_1' are just frequency offset versions of a_1, b_1 with a shift due to the C_{LO1} cable of $C_1 e^{j\varphi_{LO1}}$. This allows us to simplify the S-parameter calibration equations:

$$S'_{11} \approx \frac{b'_1}{a'_1} \approx \frac{b_1 C_1 e^{j\varphi_{LO1}}}{a_1 C_1 e^{j\varphi_{LO1}}} \qquad S'_{21} \approx \frac{b'_2}{a'_1} \approx \frac{b_2 C_2 e^{j\varphi_{LO2}}}{a_1 C_1 e^{j\varphi_{LO1}}}$$
$$S'_{12} \approx \frac{b'_1}{a'_2} \approx \frac{b_1 C_1 e^{j\varphi_{LO1}}}{a_2 C_2 e^{j\varphi_{LO2}}} \qquad S'_{22} \approx \frac{b'_2}{a'_2} \approx \frac{b_2 C_1 e^{j\varphi_{LO2}}}{a_2 C_1 e^{j\varphi_{LO2}}} \qquad (1).$$

(1) shows that cable stress on the LO cables will directly affect S_{21} and S_{12} but has little effect on S_{11} or S_{22}. To first order, S_{21} and S_{12} will change reciprocally, so taking the geometric mean, $(S'_{21}S'_{12})^{1/2} \approx \sqrt{b_1 b_2 / a_1 a_2} \approx b_2/a_1 = S_{21}$, should give a better estimate of the actual transmission. In the ideal case, S'_{21} and S'_{12} have opposite LO induced phase shifts, but practically there are non-linear amplitude shifts as well. As we can't directly measure the LO cable changes [9], we are forced to minimize phase and amplitude variations in the LO cabling [3].

C. Setup and Calibration

We align the antennas for a given antenna test and note the encoder counts for the robot, hexapod and rotator. Our alignments, once calculated and checked with the laser tracker, are mechanically repeatable to λ/50 [3]. This allows us to depend on the long-term stability of the alignments and calibrate the mmWave equipment as needed. Figure 3 shows a conceptualization of the VNA system. The LO which generates the phase and amplitude reference at mmWave, needs to be properly routed to minimize stress on the cabling [3].

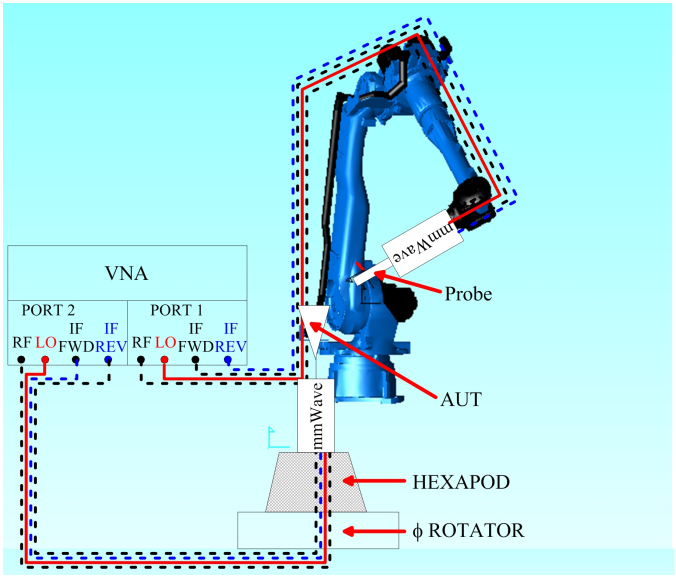

Figure 3. The RF setup of CROMMA. The LO cables (solid lines) from the VNA to the mmWave converters are the major contributors to drift due to bending and temperature.

We chose a nominally aligned position along the on-axis extrapolation path ($d \cong 75$ mm) as the unknown-thru point, Figure 4, and noted encoder counts and path to the unknown-thru point so it can be repeated with minimal robotic backlash and maximum repeatability. The calibration was then performed from 103.2503 to 133.2503 GHz in 100 MHz steps at an intermediate-frequency bandwidth (IFBW) of 100 Hz, which

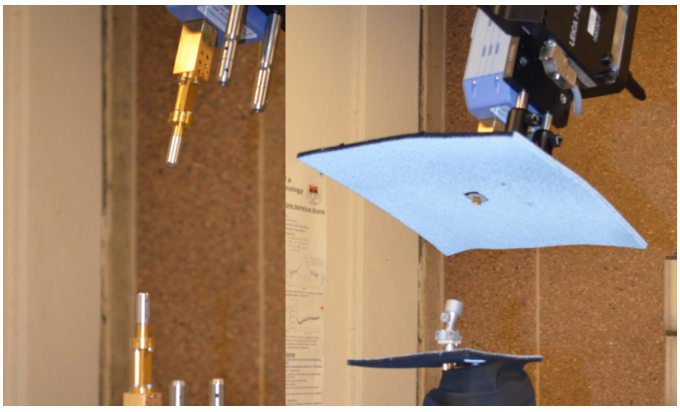

Figure 4. Calibration of the VNA on CROMMA during the AUT tests. The left shows characterization of the ports using the calibration kit standards. The right shows the "unknown-thru" at the 17 ° main beam offset and a separation of 75 mm.

yielded approximately 100 dB of flange-to-flange dynamic range. While this setup resulted in an unaliased distance of $c/\Delta f$ = 3 m, much longer than the scan distance or the anticipated unknown-thru length, it provided improved estimation of the insertion phase and delay of the unknown-thru.

III. Measurements and Results

After the broadband calibration, pattern and gain measurements were taken at the desired frequencies of 112.7503, 118.7503 and 124.7503 GHz [7].

A. Bi-directional Gain-Extrapolation

The three-antenna extrapolation method [8] can return more than the far-field gain and polarization of the antennas. Using the unknown-thru, we can also infer the free-space reflection coefficients of each antenna and attempt to assess the effects of multiple reflections [8,10]. Figure 5 shows the transmission loss between the antennas and the difference between the forward, S_{21}, and reverse, S_{12}, measurement. This difference should be ideally near zero dB, not exactly zero as the unknown-thru calibration requires measurements be taken at different times, and the probe was constantly moving. Figure 6 shows the insertion phase (and inferred distance from phase) versus separation [3]. As the phase measures relative distance, the zero error was set at 75 mm, where the unknown-thru was measured.

Figure 6 shows a 0.018 mm shift between the forward and reverse measurements. At close distances (<50 mm), the phase is taking the expected deviation from flat as the antennas are electrically very close. At far distances (>350 mm), we see deviations probably due to excessive cable flexure. In the central region, we expect to see an approximate 0.016 mm difference as the robot is moving at a 1mm/s velocity and at 100 Hz IFBW, the measurement time is approximately 2*0.8/IFBW=16 ms for the bi-directional measurement.

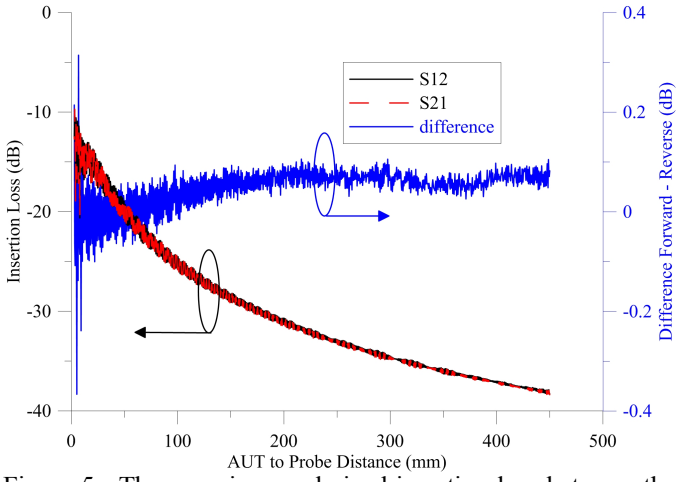

Figure 5. The on-axis co-polarized insertion loss between the AUT and the probe. Since the unknown-thru calibration requires a bi-directional measurement, we see the effect of movement and LO cable flexure on the measured transmission.

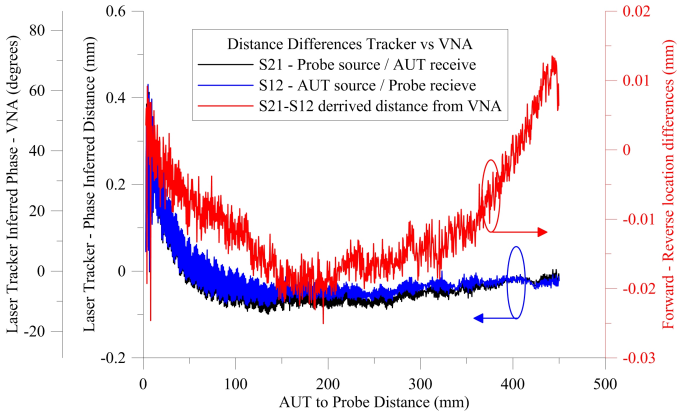

Figure 6. Comparing the insertion phase (and inferred distance) from the VNA to the direct distance by the laser tracker, as well, as the VNA inferred differences in distance using S_{21} and S_{12}.

Continuing the examinations of the extrapolation data, Figure 7 shows the reflections at both ports as distance increases. It is common to correct the extrapolated pair gain and the measured pattern in near-field scanning by the free space reflection coefficient. Measuring the actual reflections show that even at $2D^2/\lambda$, the reflections have not fully settled to a stable, much less the far-field state. So, correcting the results to just the FF, or free-space, reflection value may not remove all the near-field reflection induced errors in the final gain result [8,12].

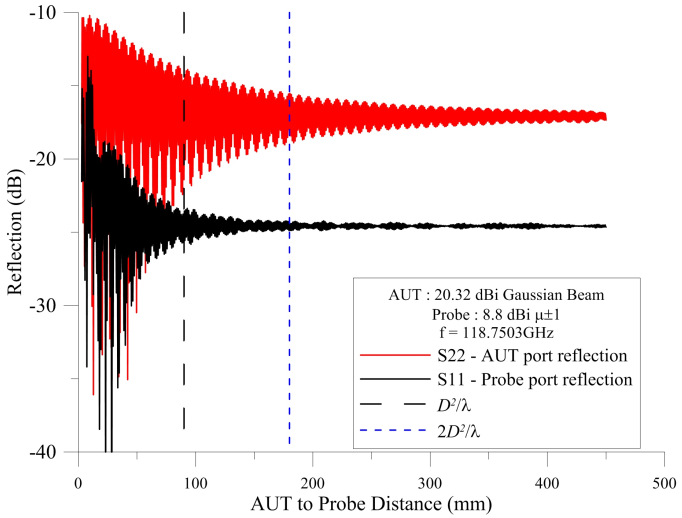

Figure 7. Examining the reflections seen by the AUT (top) and probe (bottom) as distance increases.

B. Bi-directional Pattern Measurements

The SNF scan distance of 125 mm was chosen, because during the extrapolation scans, the change in measured reflection variations seen by the probe were less than ±0.1 dB, see Fig. 7. Other measurement parameters are listed in Table I. If the reflections seen by the AUT were fully considered, the choice of scan distance may have been larger.

TABLE I. PATTERN MEASUREMNT PARAMETERS.

Parameter	Description
Frequency	112.7503, 118.7503, 124.7503 GHz
Scan Type	Spherical
Coverage	Double coverage – upper hemipshere
θ range	$-90° \le \theta \le 90°$
ϕ range	$0° \le \phi \le 360°$
Angular increment	$\Delta\phi = \Delta\theta = 1°$
Radius	125 mm
IFBW	200 Hz
Measurment time	*8 ms ≈ 2*(0.8/IFBW)* Bi-directional
Modal Analysis	$2ka_{AUT} \approx 100$ modes $\Delta\phi, \Delta\theta \approx 360$ modes, asssures oversampling
Robot velocity	10 mm/sec

C. *Examining the transmission data and pattern.*

Similar to the extrapolation data, S_{21} should equal S_{12}, however, the robot is moving. To keep our positional uncertainties low, we do not want to move the probe more than λ/50 during the primary, forward, S_{21} measurement. At 10 mm/sec, the 4 ms single direction measurement transits 40 μm or λ/62.5. This means using the laser tracker data for the reverse measurement, we can expect a systematic ~λ/30 offset. We processed the forward measurement, Figure 8, and calculated the pattern and compared it to the simulated pattern, Figure 9.

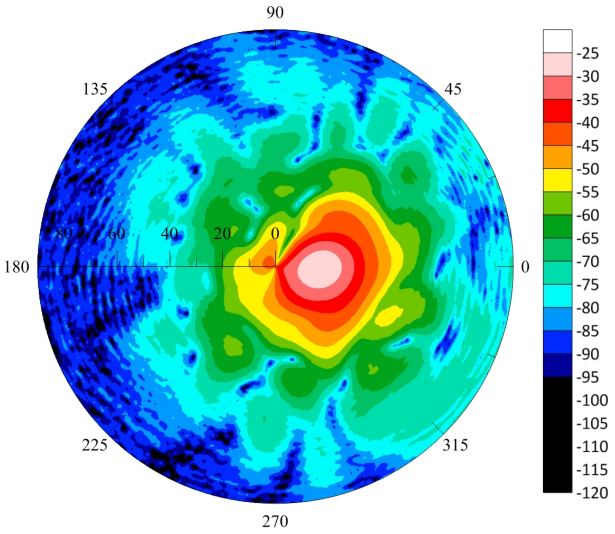

Figure 8. The on-axis co-polarized forward near-field insertion loss between the AUT and the probe.

We see both the raw near-field (NF) and far-field (FF) data, show that there is an asymmetry in the pattern. We believe that the alignment is acceptable as the FF peak lies on the ϕ=0° axis. We expected that there may be some asymmetry along θ because the 17° waveguide bend/transition may cause a non-uniform phase illumination of the aperture.

D. *Examining the reflection data*

Figure 10(a) shows the raw reflection data seen at the AUT and probe measurement ports. The raw S_{11} and S_{22} include the FF reflection of the individual antennas, as well as, the unwanted AUT-to-probe interaction and other reflections seen by the probe and AUT. We extrapolated the complex reflection data,

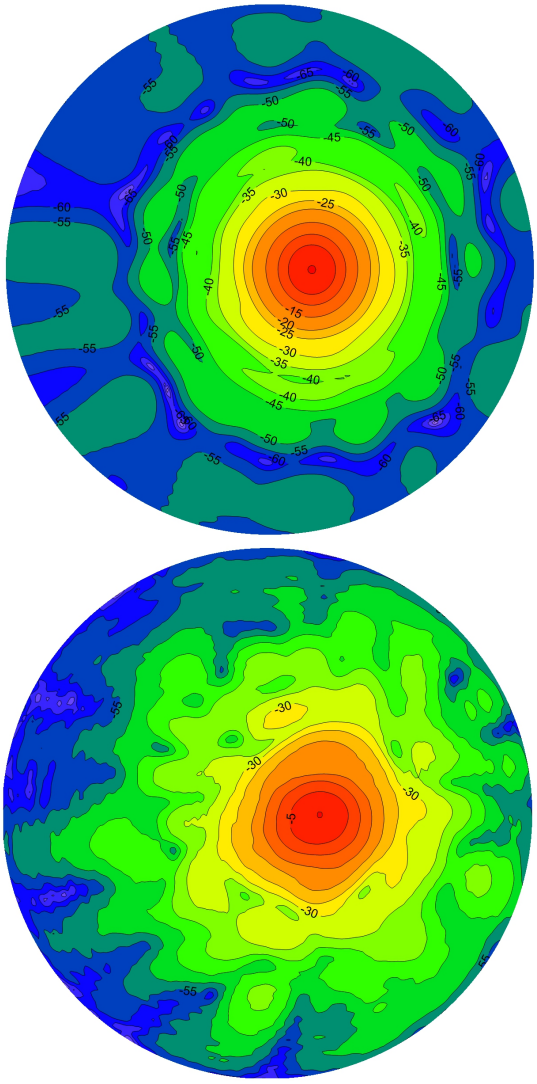

Figure 9. Simulated (top) and measured (bottom) Far-Field patterns for a WR-08 corrugated antenna.

Figure 7, to infinity to determine the free space reflection coefficient of each antenna. These values were subtracted from the reflection scan data, Figure 10(b). *While there is rather limited mathematical basis for using reflection data in the near-field to far-field (NF2FF) forward transform*, we wanted to see the results of processing the reflection data through the forward NF2FF transform, Figs. 10(c)-(d). We then examined the resultant "patterns" for qualitative analysis purposes.

The raw subtracted SNF data, Figure 10(b), show the direct horn-to-horn interaction centered at ϕ=0°, θ=17°. It also highlights alignment accuracy between the AUT and the probe. Reflections from the robot, the room, the AUT flange and mounting structure can also be seen. The FF "pattern" data, 10(c)-(d), seem to suggest that these interactions may be removed by using a limited transmission equation which includes multiple reflections [13]. We should examine the possibility that there is sufficient data to do this from the bi-directional measurement.

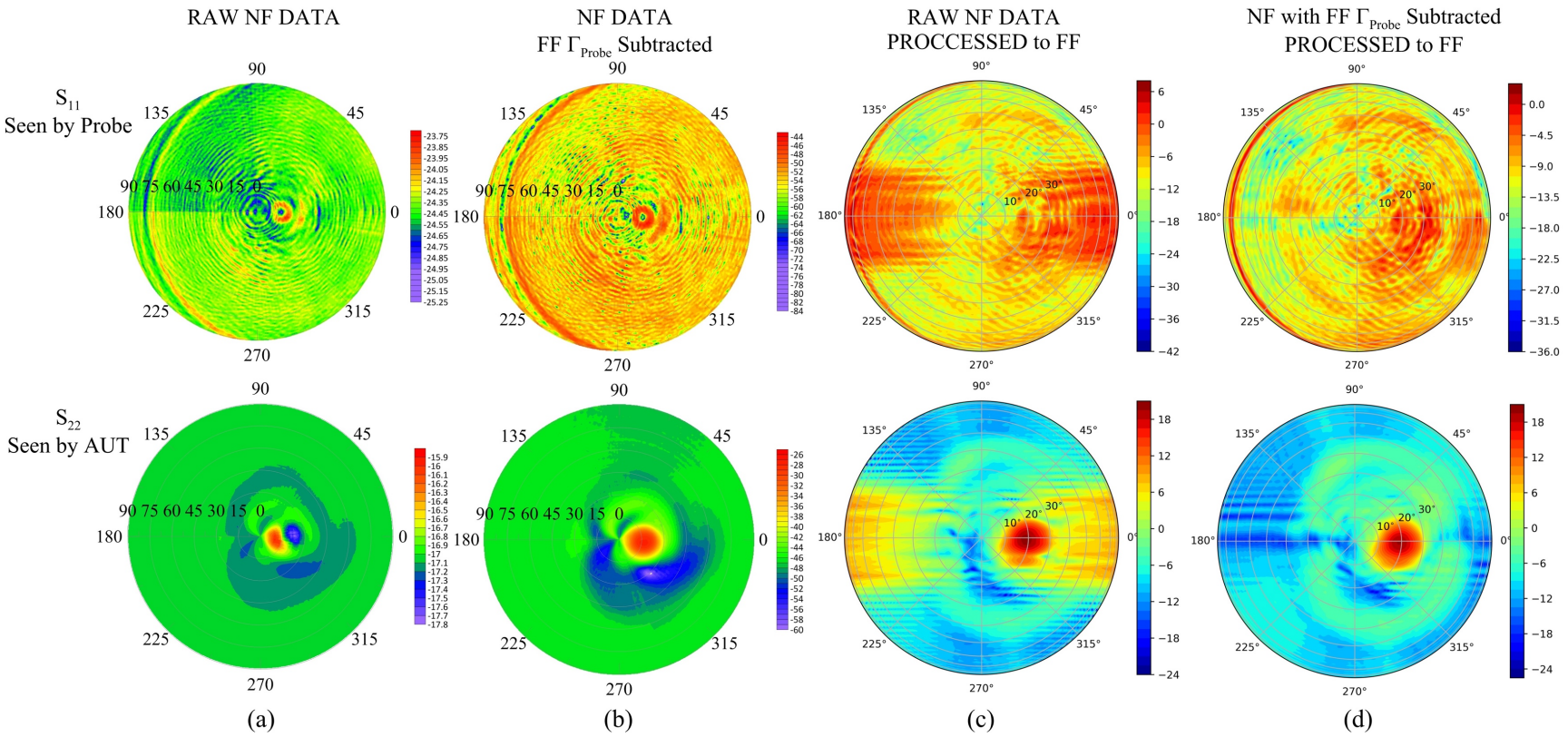

Figure 10. The reflection data as seen by the probe port (1, top) and AUT port (2, bottom) are shown in their raw form (a) and with the far-field (FF) antenna mismatch for each port subtracted (b). The AUT-to-probe interactions centered at ϕ=0°, θ=17° is more obvious as seen by the AUT versus the probe. The reflection data was then processed using the NF2FF transform as if it were transmission data. The raw reflection data transformed into the FF, (c), and the data with the antenna mismatch subtracted transformed to the FF, (d) are shown. We used the transmission measurement distance of 125mm for processing the reflection data through the NF2FF transform.

To attempt this change in the transmission equation, the subtracted SNF reflection data needs to be spatially or modally gated and the energy needs to be properly accounted for in the transmission parameter. This is an exercise for future analysis.

E. Forward versus Revese transmission data

We compare S_{21} and S_{12} in Figure 11. The difference in the forward and reverse measurements are generally less than ±0.5 dB when the signal is within 20 dB of the peak at ϕ=0°, θ=17°. If we can assume that to first order (1) holds and that the LO induced signal error is reciprocal in S_{21} and S_{12}, this can lead us to believe that the uncertainty in S_{21}, versus uncertainty the final measured result, due to cable flexure can be limited to approximately half of the difference in Figure 11 [9]. Furthermore, using the geometric mean of the forward and reverse measurements in the NF2FF transform, may result in a lower uncertainty level compared to a single-direction measurement.

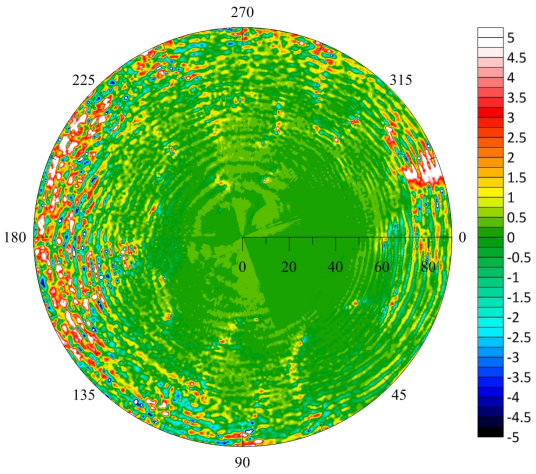

Figure 11. Difference (in dB) between S_{21} and S_{12}. Levels are less than ±0.5 dB in the region within 20 dB of the peak.

IV. Discussions and Conclusion

We performed extrapolation and SNF measurements from 112 to 125 GHz, in the WR-08 waveguide band. The inability to make a direct connection between the AUT and probe ports lead us to use the unknown-thru calibration technique to remove the systematic effects in the VNA and WR-08 extender heads. While at first glance, the disadvantages of the increased complexity over the single source/receiver setups used in many systems and the increased measurement time were troublesome, we found that insight from the additional data could be advantageous.

Especially when using harmonic mixers, LO cable changes during movement can affect measurement results. The most important insight we garnered is that, to first order, the bi-directional two-port measurement can be used to characterize and minimize the effect of LO cable changes by combining the forward and reverse measurements.

This extrapolation data show that the horn-to-horn interaction may be significant and could affect the extrapolation and NF pattern data, even though the SNF measurement radius was greater than D^2/λ at approximately 50λ.

The reflections taken during the SNF measurement can be used to assess the level of AUT-to-probe interactions and may show setup and facility imperfections. Finally, the possibility exists that there is enough information in the reflection data to reduce the AUT-to-probe interaction in the final SNF pattern data and improve the uncertainty of the SNF measurement pattern and gain results.

Acknowledgement

We would like to thank Professor Albin J. Gasiewski and the PolarCube team at the University of Colorado Space Grant Consortium for providing the feed horn, support on the systems and designs for PolarCube, and many helpful discussions.

References

[1] E. B. Larsen, R. L. Ehret, D. G. Camell and G. H. Koepke, "Calibration of antenna factor at a ground screen field site using an automatic network analyzer," *National Symposium on Electromagnetic Compatibility*, Denver, CO, USA, 1989, pp. 19–24. doi: 10.1109/NSEMC.1989.37143.

[2] M. E. Bialkowski and G. S. Woods, "Application of a six-port network to a near-field antenna measurement system," in *Electronics Letters*, vol. 21, no. 23, pp. 1066–1068, 7 November 1985. doi: 10.1049/el:19850756.

[3] D. Novotny, J. Gordon, J. Guerrieri, " Antenna Alignment and Positional Validation of a mmWave Antenna System Using 6D Coordinate Metrology." *Proceedings of the 36th AMTA*, Tuscon, AZ, USA, 2014, pp. 247–252.

[4] K. Wong, "The "unknown thru" calibration advantage," *ARFTG 63rd Conference, Spring 2004*, Fort Worth, TX, USA, 2004, pp. 73–81. doi: 10.1109/ARFTG.2004.1387858.

[5] A. Ferrero, U. Pisani and F. Sanpietro, "Save The Thru in the A.N.A. Calibration," *40th ARFTG Conference Digest*, Orlando, FL, USA, 1992, pp. 128–135. doi: 10.1109/ARFTG.1992.327007.

[6] J. A. Gordon, D. R. Novotny, M. H. Francis, R. C. Wittmann, M. L. Butler, A. E. Curtin, J. R. Guerrieri, L. Periasamy, and A. J. Gasiewski, "An All-Metal, 3-D-Printed CubeSat Feed Horn: An assessment of performance conducted at 118.7503 GHz using a robotic antenna range.," in IEEE Antennas and Propagation Magazine, vol. 59, no. 2, pp. 96–102, April 2017. doi: 10.1109/MAP.2017.2655574.

[7] R. C. Wittmann, M. H. Francis, D. R. Novotny, J. A. Gordon, M. S. Allman, "Near-Field Spherical Scanning Measurement of a 3DPrinted Horn at WR-8 Frequencies," *AMTA 2018 Proceedings*, WIlliamsburg, VA, USA, 2018.

[8] A. Newell, R. Baird and P. Wacker, "Accurate measurement of antenna gain and polarization at reduced distances by an extrapolation technique," in *IEEE Transactions on Antennas and Propagation*, vol. 21, no. 4, pp. 418–431, July 1973. doi: 10.1109/TAP.1973.1140519.

[9] D. Hess, "Principle of the three-cable method for compensation of cable varitiaon," *AMTA 1992 Proceedings*, Columbus, OH, USA, 1992, pp. 10-26–10-31.

[10] D. Kerns, Plane-Wave Scattering-Matrix Theory of Antennas and Antenna-Antenna Interactions, NBS Monograph 162, Washington, DC: US GPO, 1981, pp.27–34.

[11] J. Hansen, Spherical Near-Field Antenna Measurements, London, England: Peter Peregrinus Ltd, 1988, pp. 217–219.

[12] D. Hess, "An apparent discrepancy between impedance mismatch factors for near-field and far-field measurments," *AMTA 2005 Proceedings*, Newport, RI, USA, 2005, pp. 116–121.

[13] Ref [11], pp. 82–87.